Int. J. Electrochem. Sci., 14 **(2019)** 2693 – 2704, doi: 10.20964/2019.03.54

International Journal of
ELECTROCHEMICAL
SCIENCE
www.electrochemsci.org

Synergistic Effect between Chloride and Sulfate Reducing Bacteria in Corrosion Inhibition of X100 Pipeline Steel in Marine Environment

F. Xie[1,*], *Z. W. Guo*[1], *D. Wang*[1,*], *R. Li*[2], *M. Wu*[1], *Y. Zong*[1], *Y. C. Wang*[3]

[1] Storage and Transportation, College of Petroleum Engineering, Liaoning Shihua University, Fushun, Liaoning, 113001, China.
[2] PetroChina Liaoning Fushun Marketing Company, Fushun, Liaoning, 113006, China.
[3] PetroChina Northeast Marketing Company, Shenyang, Liaoning, 110000, China
[*]E-mail: xiefei0413@163.com, wd841015@163.com

Received: 17 October 2018 / *Accepted:* 26 December 2018 / *Published:* 7 February 2019

Large amounts of chloride ions and sulfate reducing bacteria (SRB) are present in marine environments owing to which the corrosion of subsea pipeline steel is inevitable. In this study, the influence of chloride content on the corrosion behavior of X100 pipeline steel in seawater containing SRB was investigated, using electrochemical impedance spectroscopy and potentiodynamic polarization. The adhesion and film layer state of SRB at different chloride contents were observed by scanning electron microscopy. The results show that an appropriate increase in chloride concentration is beneficial for SRB growth, but when the chloride concentration is too high, the growth of SRB is inhibited. In this study, the optimum salinity for SRB growth is found to be 35 g L^{-1}. Under the combined effect of SRB and chloride ions, with an increase in the chloride concentration, the corrosion rate of X100 pipeline steel decrease after an initial increasing trend. When the chloride concentration is 35 g L^{-1}, the metal surface film is the densest and most protective, and the corrosion rate of the specimen is minimal. This is because of the synergism between the destructive effect of chloride ions on the surface film of the electrode and the influence of chloride ions on the SRB growth process.

Keywords: X100 pipeline steel; sulfate reducing bacteria (SRB); chloride; corrosion behavior

1. INTRODUCTION

In recent years, the oil and gas industry has developed rapidly as a consequence of the continuously increasing demand for energy. Therefore, long-distance transmission of oil and gas has become necessary. To increase efficiency and reduce costs, large-scale use of high-pressure, large-

volume, and high-grade pipeline steel is necessary for the development of oil and gas pipelines [1–3]. Among such pipelines, the X100 pipeline steel is used as an advanced reserve steel; it has several advantageous characteristics such as high strength, high pressure resistance, and low cost. Hence, it is a subject of current academic research [4–6]. In addition, studies on corrosion and protection against corrosion in sea water have attracted much attention. Sea water is considered to be an environment with very complex corrosion characteristics; it contains large amounts of corrosive anions, microorganisms, and macroscopic organisms. Among them, chloride ions and sulfate-reducing bacteria (SRB) are the most common constituents [7, 8]. Therefore, corrosion of subsea pipeline steel is unavoidable and may cause environmental pollution and huge economic losses.

Owing to its small radius, the chloride ion is very aggressive and can gather preferentially in the defect areas of the metal surface, resulting in an increase in the film dissolution rate [9]. Extensive research on the corrosion of metals in chloride-containing environments has been carried out. Li showed that increasing the chloride concentration in sea water can promote the pitting corrosion of aluminum alloys [10]. Shi showed that, with an increase in the chloride concentration from 1% to 4%, the corrosion rate of 316L stainless steel increases initially and thereafter decreases [11]. Zhang et al. discussed the effect of chloride ions on the corrosion of stainless steel in a H_2S/CO_2 environment [12]. It is believed that as the chloride concentration increases, the corrosion potential shifts negatively and the activation and dissolution of the anode are accelerated, which can be attributed to the penetration and absorption effects of chloride ions. Additionally, microbial corrosion is a research topic within the scope of metal corrosion. When a metallic material is immersed in sea water, bacteria are gradually adsorbed on the metal surface, and their life activities and metabolites can easily change the surface state and local micro-environment of the metal, thereby affecting the corrosion process of the metal in a marine environment [13–15]. The chloride concentration reflects the salinity of a medium. Salts can change the osmotic pressure of microorganisms, affect the transport of bacterial substances, and change the activity of microorganisms. Therefore, an appropriate salinity is beneficial for the growth and reproduction of bacteria; at the same time, excess salt content leads to the separation of the cytoplasmic wall, eventually causing cell dehydration or even death [16–18]. However, SRB has a strong survival adaptability. Wu et al. studied the effect of salinity on the growth of SRB and determined that a high salinity can inhibit the growth of SRB. However, SRB is still viable at a NaCl concentration of 50 g L^{-1} [19].

Extensive research has been conducted worldwide on the independent effects of microbes or chloride ions on metal corrosion and preliminary results has been obtained. However, the marine environment is very complicated. SRB and chloride ions coexist and chloride content is an important factor influencing the microbiological corrosion of metals. There are only a few reports on the effect of chloride content in sea water on microbiological corrosion and the specific reaction mechanism has not yet been elucidated. Therefore, in this study, the X100 pipeline steel was selected as the research subject and the influence of chloride content on its corrosion behavior in sea water containing SRB was investigated using electrochemical impedance spectroscopy (EIS), potentiodynamic polarization, and scanning electron microscopy (SEM). This study provides some theoretical references for the application of high-strength pipeline steels in an actual marine environment and for the prevention of microbiological corrosion.

2. EXPERIMENTAL DETAILS

2.1. Experimental materials

The X100 pipeline steel was used as the specimen material; its chemical composition is presented in Table 1. The steel was processed into two sizes – an electrochemical specimen of dimensions 10 mm × 10 mm × 2 mm soldered to a copper wire and packaged in polytetrafluoroethylene with epoxy resin, leaving a circular working area of 1 cm^2 and an immersion specimen of dimensions 20 mm × 10 mm × 2 mm, punched with a round hole at one end. All the specimens were washed with acetone and thereafter ground with a waterproof abrasive paper step-by-step from 80-grit to 2000-grit, cleaned with ethanol and distilled water, and finally stored in a desiccator for use.

Table 1. Chemical composition of X100 steel (wt.%)

Steel	C	Si	Mn	P	S	Mo	Fe
X100	0.04	0.2	1.5	0.011	0.003	0.02	Bal.

2.2. Experimental solution

The experimental solution was simulated in the environment of South China Sea. According to the data range of the environment of South China Sea, deionized water was used to prepare the simulation solution with NaCl mass fractions of 5, 20, 35, and 50 g L^{-1}. The SRB used in this experiment was obtained from the South China Sea by the separation and purification of sea mud. The liquid culture medium consisted of two parts – culture medium I and culture medium II. The composition of culture medium I was 0.5 g L^{-1} K_2HPO_4, 0.5 g L^{-1} Na_2SO_4, 1 g L^{-1} NH_4Cl, 0.1 g L^{-1} $CaCl_2$, 2 g L^{-1} $MgSO_4.7H_2O$, 1 g L^{-1} yeast extract powder, and 3 mL of $C_3H_5O_3Na$. The pH of culture medium I was adjusted to 7.2 with a 4% NaOH solution; subsequently, it was sterilized in a pressure steam sterilizer for 15 min, and then allowed to stand at room temperature. The composition of culture medium II was 0.1 g L^{-1} ascorbic acid, 0.1 g L^{-1} $Na_2S_2O_4$, and 0.1 g L^{-1} $(NH_4)_2Fe(SO_4)_2$ $6H_2O$. Culture medium II was sterilized using ultraviolet radiation through a cylindrical filter and it was later mixed with the culture medium I at a ratio of 1:1. The mixed solution was used as the liquid culture medium. The SRB liquid culture medium and the sterilized simulated solutions with four chloride concentrations were evenly mixed at a ratio of 1:1, after which 1% of the total amount of pure bacteria (pure bacteria of constant-temperature culture for four days) was added; thus, four types of experimental solutions were obtained. Moreover, N_2 (99.9% purity) was added to the sterilized simulation solutions for approximately 30 min before mixing in order to ensure an anaerobic environment for SRB growth.

2.3. Charts of the SRB growth cycle

An optical densitometry method (OD) method was used to plot the growth charts of SRB in the experimental simulation solutions. For 14 days, the experimental solutions of different chloride

concentrations were extracted. Sterilized sea water solutions with four chloride concentrations were used for comparison. The absorbance (Abs) was measured using a UV-2550 ultraviolet spectrophotometer. As the absorbance was within the test range of 0.15–1.0, which is approximately equal to the OD value, the curve of SRB growth in a cycle was obtained by measuring the OD value.

2.4. Electrochemical measurements

The X100 steel specimens were sealed and immersed in the experimental solutions with chloride ion concentrations of 5, 20, 35, and 50 g L^{-1} for 14 days, and thereafter tested using a PARSTAT2273 electrochemical workstation. The experiment used a conventional three-electrode configuration. The X100 steel specimen (1 cm^2 size) was used as the working electrode, while graphite and saturated calomel electrode (SCE) were used as the auxiliary and reference electrodes, respectively. EIS tests were performed at an open circuit potential from 0.01 Hz to 100 kHz at AC amplitude of 10 mV and the corresponding results were analyzed using ZSimpWin software. Before conducting EIS measurements, the open circuit potentials were recorded continuously for 1 h. Finally, potentiodynamic polarization curves were generated from −1.2 V to 0 V at a scan rate of 0.667 mV s^{-1} and the corresponding results were fitted and analyzed using Origin software. The experimental temperature was maintained at room temperature and all the potentials were relative to SCE.

2.5. SEM analysis

The X100 steel surface was examined on an ultraviolet operation table after exposing the specimen to the experimental solutions of different chloride concentrations for 14 days. Each specimen was first soaked in a 5% glutaraldehyde solution for 2 h and thereafter in ethanol solutions with volume fractions of 50%, 70%, and 100% for 15 min for successive dehydration. Finally, the corrosion morphology of the soaked specimens was observed and analyzed using SEM.

3. RESULTS

3.1. Growth of SRB at different chloride concentrations

The growth charts of SRB at four chloride concentrations are presented in Fig. 1. As shown in the figure, over days 1–4, SRB exhibited an exponential growth due to an abundance of nutrients in the solution. During days 5–10, a stable growth phase was observed; owing to the gradual consumption of nutrients in the solution, the rates of reproduction and decline of SRB were the same, and the number of SRB was relatively stable. During days 11–14, a declining stage was observed; owing to a lack of nutrients and living space, the number of dead SRB increased and the number of active SRB decreased. With an increase in the chloride concentration, the number of SRB increased initially and then decreased. At a chloride concentration of 35 g L^{-1}, the number of SRB was the highest.

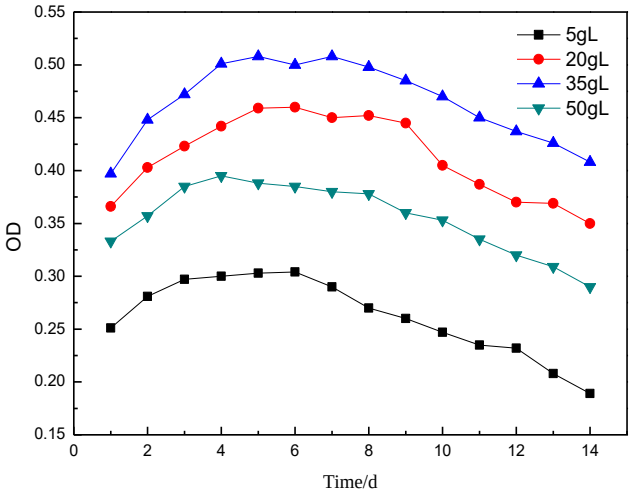

Figure 1. Growth chart of SRB in experimental solutions of different chloride concentrations

3.2. Electrochemical impedance spectroscopy

The results of EIS analysis on X100 steel specimens immersed in the experimental solutions of different chloride concentrations for 14 days are shown in Fig. 2. It is can be observed that the EIS pattern in all the experimental solutions exhibited a single capacitive reactance arc, indicating that the electrochemical reaction is affected by the electrode process. The diameter of the capacitive reactance arc reflects the rate of the electrochemical reaction [20]. As shown in the figure, the diameter of the arc initially increased and then decreased beyond a certain chloride concentration. This suggested that the corrosion rate of X100 steel decreased at first and then increased with an increase in chloride concentration. When the chloride concentration increased to 35 g L^{-1}, the corrosion rate was minimum.

In this study, an equivalent circuit model (Fig. 3) was selected and the EIS results were fitted using ZSimpWin. Here, R_s and R_f represent the solution resistance and surface layer resistance, respectively. The impedance of the regular phase-angle element Q is $Z_{CPE} = Y_0^{-1}(jw)^{-n}$, which is related to the dielectric properties of the corrosion product layer. The value of n ($0<n<1$) reflects the roughness of the metal surface. Q_f and Q_{dl} are the surface layer capacitance and interface double-layer capacitance, respectively. R_{ct} represents the charge transfer resistance, which reflects the corrosion rate of the metal; the larger its value, the lower the metal corrosion rate. The fitted electrochemical parameters are listed in Table 2. It can be observed that the solution resistance R_s does not change significantly, indicating that the environmental conductivity is relatively stable [21, 22].

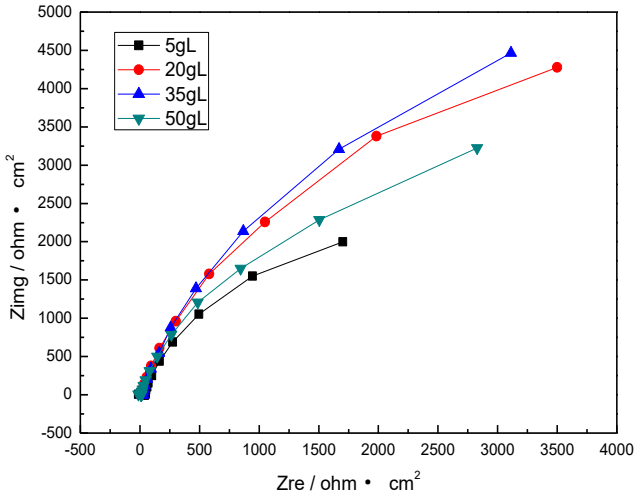

Figure 2. Nyquist plots of X100 steel in experimental solutions of different chloride concentrations

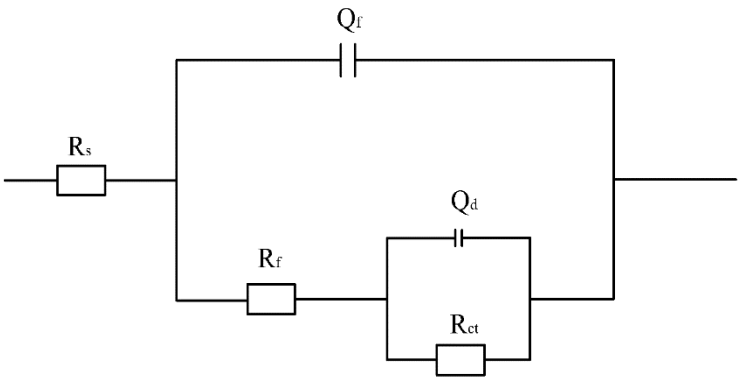

Figure 3. Equivalent circuit model of X100 steel in experimental solutions of different chloride concentrations

Table 2. Fitted electrochemical parameters of X100 steel in experimental solutions of different chloride concentrations

Cl^-(g L^{-1})+ SRB	R_s ($\Omega.cm^2$)	Q_f ($\mu F.cm^{-2}$)	R_f ($\Omega.cm^2$)	Q_{dl} ($\mu F.cm^{-2}$)	R_{ct} ($\Omega.cm^2$)
5	41.14	0.002765	124.2	0.001075	9360
20	20.54	0.001119	99.01	0.000673	16520
35	14.14	0.0009033	16.58	0.000255	18460
50	11.38	0.000524	3.845	0.001079	11460

At chloride concentrations of 5, 20, 35, and 50 g L^{-1}, the charge transfer resistance R_{ct} of the specimen was 9360, 16520, 1860, and 11460 Ω, respectively. Thus, R_{ct} initially increased and then decreased with an increase in chloride concentration. When the chloride concentration increased to 35 g

L^{-1}, the charge transfer resistance R_{ct} reached the highest value, indicating that the X100 steel exhibited the lowest corrosion rate at this point.

3.3. Potentiodynamic polarization

The results of potentiodynamic polarization tests of the X100 steel specimens immersed in experimental solutions of different chloride concentrations for 14 days are shown in Fig. 4. It can be observed from the figure that the anodic polarization curve exhibited an activated state at a chloride concentration of 5 g L^{-1}. Further, it gradually shifted from the activated state to a passivated state at chloride concentrations of 20 g L^{-1} and 35 g L^{-1}. At a chloride concentration of 35 g L^{-1}, the passivated interval of the curve increased and the passivation became more obvious. At a chloride concentration of 50 g L^{-1}, the passivated state weakened and the curve showed a shift from activation to passivation. It could be observed that with an increase in chloride concentration in the solution, the stability of the passivation film formed on the surface of X100 steel initially increased and then decreased. This may be attributed to the combined effect of chloride ions and SRB biofilm on the metal surface.

The corrosion parameters related to polarization curves are shown in Table 2. It can be observed that the corrosion current density of X100 steel initially decreased and then increased with an increase in the chloride concentration in the experimental solutions. Therefore, the corrosion rate of the X100 steel decreased initially and then increased. At a chloride concentration of 35 g L^{-1}, the corrosion rate of X100 steel was minimum and the degree of corrosion was the lowest. This observation is consistent with the EIS results.

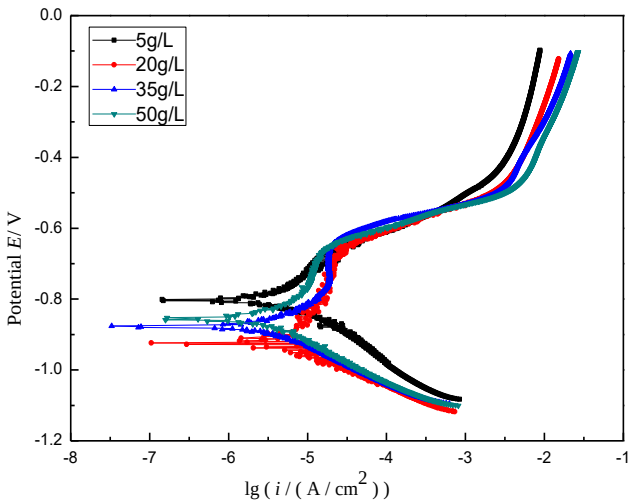

Figure 4. Polarization curves of X100 steel in experimental solutions of different chloride concentrations

Table 3. Corrosion parameters related to polarization curves

Cl^- (g L^{-1})	Icorr/(A cm^{-2})	Ecorr/V
5	6.016	-0.801
20	4.019	-0.924
35	3.514	-0.876
50	5.491	-0.858

3.4. SEM analysis

Fig. 5 shows the SEM morphology of X100 steel specimens immersed in four different experimental solutions for 14 days. From the figure, it can be observed that at a chloride concentration of 5 g L^{-1}, a layer of SRB biofilm is formed on the surface of the metal specimen, and some of the biofilm and corrosion products are mixed with each other. The thickness distribution of the biofilm is not uniform and compact; hence, it provides poor protection to the metal. At a chloride concentration of 20 g L^{-1}, the film on the metal surface is more uniform and the protective effect is enhanced. At a chloride concentration of 35 g L^{-1}, the film is adsorbed uniformly and densely on the surface of the steel, thus providing effective protection to the metal and improving its corrosion resistance. At a chloride concentration of 50 g L^{-1}, the corrosion products become rough, the film cracks, and the protective effect is reduced.

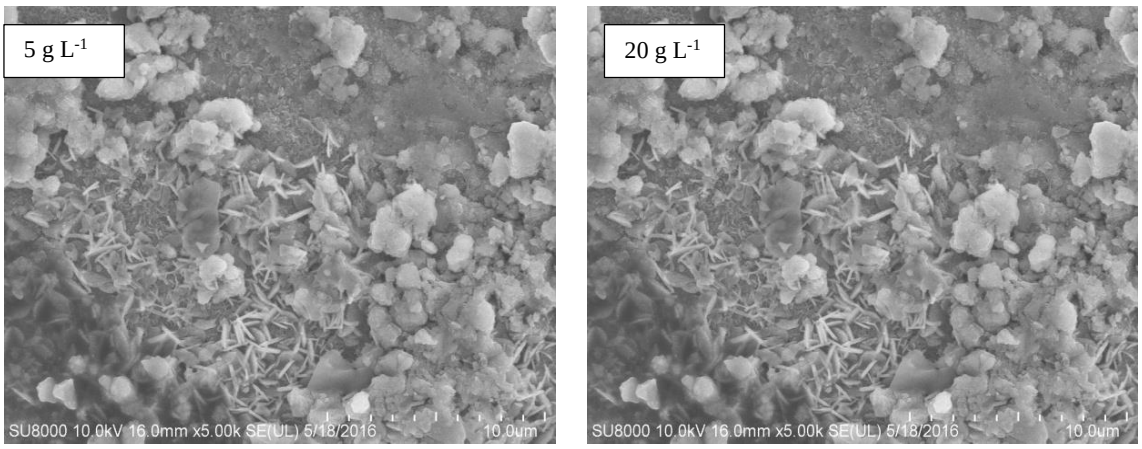

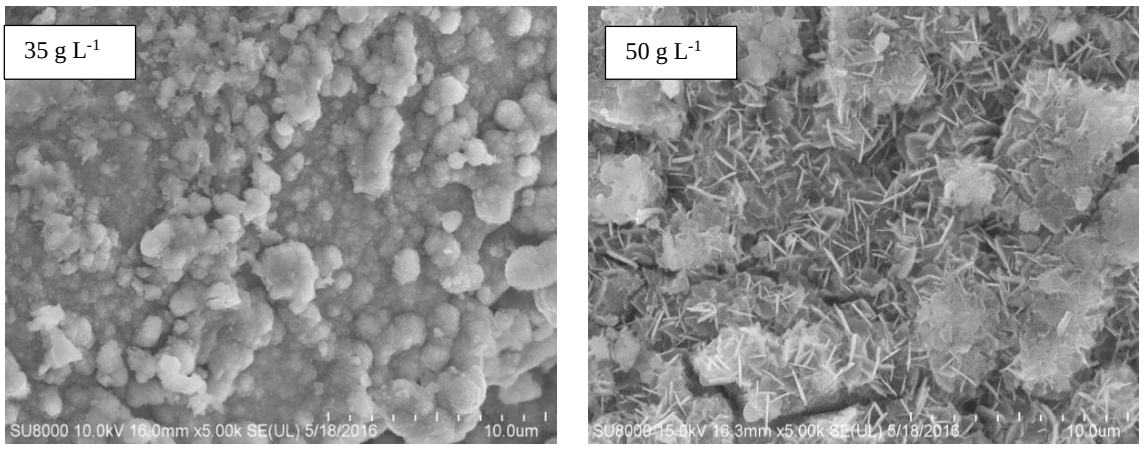

Figure 5. SEM morphology of X100 steel immersed in four different experimental solutions for 14 days

4. DISCUSSION

Sea water is an extremely complex environment with large amounts of corrosive anions and various microorganisms and macroscopic organisms. Among them, Cl^- and sulfate-reducing bacteria are the most important; therefore, the corrosion of submarine pipeline steel is mainly caused by these two factors.

4.1 Role of Cl^- in SRB present in sea water in the corrosion process of X100 steel

Cl^- present in sea water exert two effects. From the above described experimental results, it is understood that the rate of metal corrosion is accelerated as the Cl^- concentration is increased from 5 g L^{-1} to 35 g L^{-1}. This is due to the fact that X100 steel contains incomplete crystal lattices such as grain boundaries and dislocations. The weak surface of this metals is most likely to adsorbs Cl^- and other anions which have strong bonds with Fe^{2+}[23]. Cl^- can destroy the metal surface film. Exposure to fresh metals and contact with the solution promotes the corrosion reaction [24]. In addition, Cl^- will also have an effect on the growth of SRB. As shown in Fig. 1, as the concentration of Cl^- increases, the growth activity of SRB initially increased and then decreased. Cl^- reflects the salinity of a medium; as the salinity increases, the osmotic pressure of SRB in solution increases; the growth environment of SRB should have an osmotic pressure approximately equal to that of its cells. In a low osmotic pressure solution, water permeates into the cells, resulting in cell swelling or even rupture. In a high osmotic pressure solution, water will pass through the cell membrane into the solution surrounding the cell, causing cell plasmolysis and dehydration or even death [18]. In an isotonic solution, the metabolic activity of SRB is maximum; the cells neither shrink nor expand, and their original shape remains unchanged. It can be observed that an appropriate increase in Cl^- content will promote the growth of SRB, but when the Cl^- content exceeds the critical value, the growth of SRB will be inhibited. In this study, the critical value is 35 g L^{-1}.

4.2 Role of SRB in the corrosion process of X100 steel

The effect of SRB on metal corrosion can be observed from Fig. 6. There is a layer a dense or a sparse surface film on the metal surface. This may be because SRB tend to adhere to the surface of an object and can form a biofilm on the metal surface. The membrane itself has physical obstruction, which reduces the probability of Cl^- immersion on the metal surface and slows down the corrosion process of the metal [25]. In addition, microbial metabolite sulfides are filled into the pores of the microbial membrane to further strengthen the physical barrier presented by the microbial membrane [26].

4.3 Synergistic effect of between Cl^- and SRB on the corrosion behavior of X100 steel

At a Cl^- concentration of 5 g L^{-1} (Fig. 6a), according to the electrochemical test results, X100 steel exhibited a R_{ct} value of 9360 Ω cm^2 and a corrosion current density of 6.01 μA cm^{-2}. The polarization curve indicates an activated state. Owing to the small number of SRB, the biofilm formed on the metal surface is sparse and some of the biofilm is mixed with the corrosion products, resulting in a less dense metal surface film. Defects in the surface film allow the possibility of Cl^- intrusion; at this time, Cl^- plays a leading role in the erosion of the metal surface, thus promoting the dissolution of metal anodes.

The electrochemical reaction mechanisms during the experiment are as follows:

Cathodic reaction [27]:

$$2H_2O + 2e = 2H + 2OH^- \quad (1)$$

$$SO_4^{2-} + 8H = S^{2-} + 4H_2O \quad (2)$$

Anodic reaction:

$$Fe = Fe^{2+} + 2e \quad (3)$$

The corrosion reactions are as follows:

$$Fe^{2+} + S^{2-} = FeS \quad (4)$$

$$2Fe^{2+} + 6OH^- = 3Fe(OH)_2 \quad (5)$$

With an increase in the Cl^- concentration to 20 g L^{-1} (Fig. 6b), the diameter of the capacitive reactance arc increases and the corrosion current density decreases. The polarization curve gradually shifts from activation to passivation and the film becomes more uniform. This is because as the Cl^- concentration increases, the number of SRB increases; as the SRB increasingly gather on the metal surface, the biofilm becomes denser. Defects on the surface of the membrane are reduced， after which the possibility of Cl^- eroding the metal surface is reduced. At this time, the protective effect on the metal increases and the corrosion weakens.

When the Cl^- concentration increases to 35 g L^{-1} (Fig. 6c), the diameter of the capacitive reactance arc continues to increase and the corrosion current density decreases. The passivation interval of the polarization curve increases and the passivation becomes more apparent. The film layer is adsorbed on the steel surface uniformly and densely. This is because this Cl^- concentration is the most suitable for SRB growth; the number of SRB is the highest and the life activities of SRB are the most vigorous. Thus, a dense biofilm and corrosion product film are formed on the surface of the specimen,

hindering the transfer of the interface and greatly reducing the possibility of Cl^- aggregation intrusion and the protective effect of the biofilm on the metal is enhanced.

When Cl^- concentration increases to 50 g L^{-1} (Fig. 6d), the diameter of the capacitive reactance arc decreases and the corrosion current density increases. The polarization curve shifts from activation to passivation and the passivation weakens. The film shows cracks and the metal corrosion rate increases. This may be because on the one hand, Cl^- captures oxygen at the surface of the passivation film, thus breaking the passivation film and resulting in an acceleration in the corrosion process. On the other hand, as the Cl^- concentration continues to increase, the number of SRB decreases. The biofilm ruptures, and the surface of X100 steel gradually changes from biofilm to corrosion product film. The corrosion product film also becomes loose and easily falls off. A concentration difference battery is formed on the surface of the specimen, which promotes metal corrosion. Therefore, an increase in the Cl^- concentration in this process promotes corrosion.

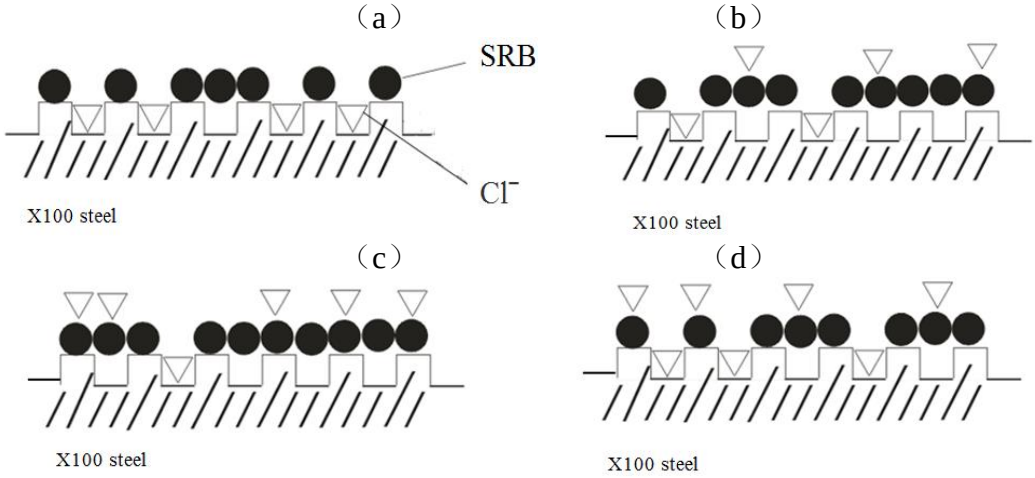

Figure 6. Distribution of Cl^- concentration and SRB on the surface of X100 steel. (a) 5 g L^{-1}, (b) 20 g L^{-1}, (c) 35 g L^{-1}, (d) 50 g L^{-1}

5. CONCLUSIONS

(1) Electrochemical measurements and SEM results show that, with an increase in the Cl^- concentration in the experimental solution, the number of SRB initially increased and then decreased. The corrosion rate of X100 steel first decreased and later increased. At a Cl^- concentration of 35 g L^{-1}, the SRB activity is the strongest, the metal surface film is the densest resulting in the best protection, and the corrosion rate of the specimen is the lowest.

(2) The corrosion behavior of X100 steel in this experimental solution system is affected by the synergism between the strong corrosive effect of Cl^- and the protective effect of the SRB biofilm. On one hand, an increase in the Cl^- content accelerates destruction of the metal surface film and promotes corrosion; on the other hand, it affects the growth of SRB as well as the protection provided by the biofilm to the steel.

(3) In actual marine environment conditions, SRB and Cl^- coexist. In order to reduce the risk of leakage accidents caused by the corrosion of subsea pipeline steel, the pipelines should be laid in the sea water areas where the Cl^- concentration is in the range of 30 g L^{-1} to 40 g L^{-1} in order to ensure the strongest SRB activity and enhance the protective effect of the biofilm on the pipeline steel.

ACKNOWLEDGEMENTS
The authors gratefully acknowledge the support by the National Science Foundation of China (grant no. 51604150 and 51574147) and Science Research Foundation of Liaoning Province (grant no. L2017LQN016).

References

1. Z. Y. Liu, Q. Li, Z. Y. Cui, W. Wu, Z. Li, C. W. Du and X. G. Li, *Constr. Building Mater.*, 148 (2017)131.
2. Z. Q. Shi, X. Y. Zhang, Y. F. Wang, M. X. Liu, K. Tang, S. S. Si and H. Li, *J. Chin. Univ. Petrol. (Edit. Nat. Sci.)*, 40(2016)128.
3. M. Jiang, *Shanghai University*, China, 2015.
4. H. Liang and J. Liu, *Mater. Lett.*, 222 (2018)196.
5. H. M. Ha, I. M. Gadala and A. Alfantazi, *Electrochim. Acta*, 204(2016)18.
6. E. Mahdi, A. Rauf and E. O. Eltai, *Corros. Sci.*, 83(2014)48.
7. Y. F. Qi, C. C. Dong and W. G. Yang, *Tot. Corros. Contr.*, 31(2017)24.
8. Q. Li, J. Wang, X. Xing and W. Hu, *Bioelectrochemistry*, 122(2018)40.
9. K. Hyun, M. Han and S. Kim, *Surf. Rev. Lett.*, 24(2017)1.
10. T. Li, X.G. Li, C. F. Dong, J. L. Zhou, T. C. Feng and J. Wu, *J. Univ. Sci. Technol. B.*, 31(2009)1576.
11. Y. H. Shi, Y. Yu, P. Liang, F. Liu and X. L. Guan, *Mater. Prot.*, 48(2015)29.
12. N. Y. Zhang, D. Z. Zeng, G. Q. Xiao, J. F. Shang, Y. Z. Liu, D. Long, Q.Y. He and A. Singh, *J. Nat. Gas Sci. Eng.*, 30(2016)444.
13. F. Liu, J. Zhang, C. Sun and B. Hou, *Corros. Sci.*, 83(2014)375.
14. D. X. Sun, M. Wu and F. Xie, *Mater. Sci. Eng., A*, (2018)721.
15. H. Y. Chen, X. Li, X. Y. Zhang, P. M. Chen and J. Yu, *Chin. J. Nonferrous Met.*, 4(2015)1080.
16. S. Chen and D. Zhang, *Corros. Sci.*, 136(2018)275.
17. Z. Xin, *Yan Tai Univerisity*, China, 2014.
18. K. R. Blight and D. Ralph, *Hydrometallurgy*, 73(2004)325.
19. W. F. Wu, B. Liu, H. J. Li, S. Li and Z. Z. Chen, *Chin. J. Environ. Eng.*, 5(2011)2527.
20. Y. Wang, G. Cheng, W. Wu, Q. Qiao, L Li and X. F. Li, *Appl. Surf. Sci.*, 349(2015)746.
21. F. L. Liu, S. T. Zhang, J. Zhang and W. H. Li, *Chin. J. Mater. Res.*, 24(2010)411.
22. I. M. Gadala and A. Alfantazi, *Corros. Sci.*, 82(2014)45.
23. J. M. Xiao and C. N. Cao, *Bejing: Chemical Industry Press*, (2004)46.
24. X. X. Song, J. Zhang, D. F. Yang and J. Z. Duan, *J. Mater. Eng.*, 3(2013)58.
25. E. Huttunen-Saarivirta, P. Rajala, L. Carpén, *Electrochim. Acta*, 203(2016)350.
26. C. M. Xu, X. Zhang, L. H. Luo and D. P. Yang, *J. Iron & Steel Res.*, 29(2017)562.
27. T. Liu, Y. F. Zhang, X. Chen, D. Wang and Y. Chen, *J. Chin. Soc. Corros. Prot.*, 34(2014)112.